Hindawi
Journal of Nanomaterials
Volume 2019, Article ID 7232715, 11 pages
https://doi.org/10.1155/2019/7232715

Research Article

Borax-Cross-Linked Guar Gum-Manganese Dioxide Composites for Oxidative Decolorization of Methylene Blue

Rohan S. Dassanayake,[1,2] Erandathi Rajakaruna,[1] and Noureddine Abidi[1]

[1]*Fiber and Biopolymer Research Institute, Department of Plant and Soil Science, Texas Tech University, Lubbock, TX 79409, USA*
[2]*Department of Chemistry, Ithaca College, Ithaca, NY 14850, USA*

Correspondence should be addressed to Noureddine Abidi; noureddine.abidi@ttu.edu

Received 16 July 2018; Accepted 13 November 2018; Published 31 January 2019

Academic Editor: Paulo Cesar Morais

Borax-cross-linked guar gum-manganese dioxide (GGB-MnO_2) composite was synthesized using an environmentally friendly synthesis route and investigated for its efficiency of decolorizing methylene blue (MB) dye solution by an ultraviolet-visible (UV-Vis) spectrophotometric study. The GGB-MnO_2 composite was characterized using X-ray diffraction (XRD), field emission scanning electron microscopy (FESEM), energy-dispersive X-ray (EDX) spectroscopy, Fourier-transform infrared (FTIR) spectroscopy, and thermogravimetric analysis (TGA). The composite (1.2 g/L) exhibited excellent oxidative decolorization of MB (30 mg/L, 50 mL) solution to over 99% in 6, 13, and 40 min at pH 4, 7, and 10, respectively. The complete decolorization of MB occurred via a catalytic adsorption-oxidation-desorption mechanism. The GGB-MnO_2 composite showed very good reusability and was stable after ten successive cycles with negligible losses of the decolorization efficiency.

1. Introduction

Industries including textile, paper, printing, leather, and paint use excessive amounts of water for processing and have the potential to contaminate waterways through the discharge of organic dyes into natural water resources and water treatment systems. Over 10000 different textile dyes with an estimated annual production of over 7×10^5 tons are available commercially [1]. Most of these organic dyes are excessively used and 10–20% are directly discharged as aqueous effluents into different water bodies [2]. Discharging of organic dyes into water bodies has raised both acute and chronic concerns to the ecosystems and human health. For example, the release of those organic dyes can give rise to eutrophication, nonaesthetic pollution, and imbalance in the aquatic biological systems and also causes chronic toxicity, carcinogenicity, and neurotoxicity towards humans and animals. In fact, the presence of a very low concentration of dye in water (>1 mg/L for some dyes) is highly visible and enough to introduce an aesthetic problem [3].

Organic dyes are mainly categorized as anionic, cationic, and nonionic dyes [4]. The major anionic dyes are divided into direct, reactive, and acid dyes, and the most problematic ones are the brightly colored, water-soluble reactive, and acid dyes as these dyes cannot be removed through conventional treatment systems. The cationic dyes are basic dyes including anthraquinone disperse, azo, and reactive dyes. Anthraquinone-based dyes are bioaccumulative and resistant to degradation due to their fused aromatic ring structure. Nonionic dyes are disperse dyes that do not ionize in the aqueous environment. Organic dyes consist of chromophores and auxochromes where chromophores determine the color of the dye while the auxochromes determine the intensity of the color [5]. Methylene blue (MB) is a heterocyclic cationic dye, used extensively in textile, leather, and paper industries. The existence of MB in wastewater can cause vomiting, profuse sweating, nausea, diarrhea, permanent burn effects of the eye, mental health disorder, and methemoglobinemia [6, 7]. Hence, the remediation of industrial wastewater is imperative before it becomes detrimental

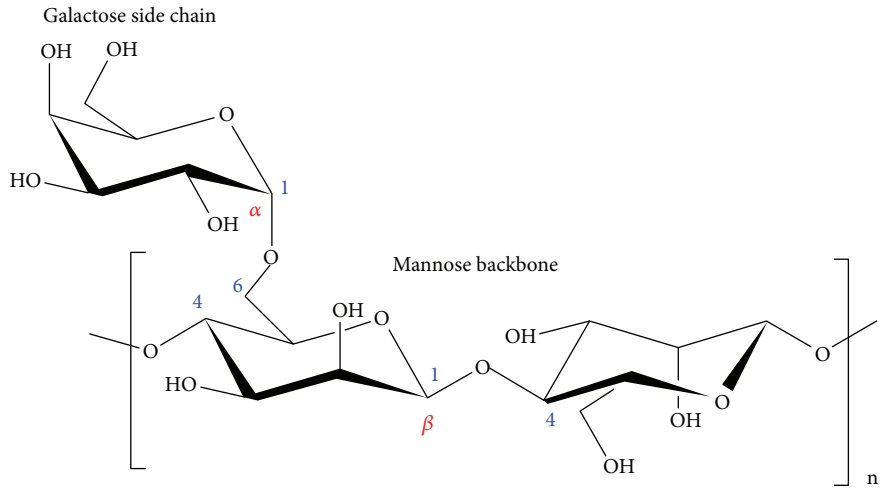

Figure 1: Structure of guar gum.

to the biological systems. At present, there is a critical need of research that enables new means of inexpensive, reusable, environmentally, and energetically sustainable wastewater management systems for wastewater treatment.

Commonly investigated technologies for removing organic dyes from wastewater include chemical precipitation and adsorption [8, 9], electrochemical oxidation and reduction [10], aerobic and anaerobic treatment [11, 12], coagulation and flocculation [13, 14], membrane separation [15], ultrafiltration [16], H_2O_2/ultraviolet (UV) and photocatalysis [17–19], ion exchange [20], sonochemical degradation [17], Fenton and heterogeneous Fenton-like catalysis [21–23], and electrolysis [24]. However, many of these methods are accompanied by various constraints such as sludge generation, adsorbent regeneration, membrane fouling, high operational cost, long operational time, and ineffectiveness in the complete removal of polycyclic aromatic compounds. Recently, new oxidation processes including advanced oxidation processes (AOPs) have attracted interests as emerging alternative techniques for the treatment of industrial effluents [25, 26]. These processes are involved in highly reactive species which have high redox potentials and, hence, can cause complete destruction of organic pollutants from wastewater [25]. Moreover, oxidation processes also show many advantages over conventional techniques including no sludge disposal, one-step decolorization and complete degradation of organic pollutants into small ions, large reactivity, low cost, minimal handling, and reusability.

Metal oxide nanoparticles (NPs) such as titanium dioxide (TiO_2) [18, 27], zinc oxide (ZnO) [28], nickel oxide (NiO) [29], cerium dioxide (CeO_2) [30], copper oxide (CuO) [30, 31], and manganese oxides (MnO_x) [32] have been widely studied in oxidation processes. Among those, MnO_x NPs have attracted special attention for the removal of organic dyes due to their unique structure and physicochemical properties [32, 33]. MnO_x are ubiquitous, nontoxic, highly reactive catalysts present in soils and sediments, desert varnishes, rock dendrites, freshwater bodies, and ocean floors [32]. MnO_x are among the strongest oxidants in natural environment with high reducing potential between 1.27 and 1.50 V [34]. Hence, MnO_x are capable of oxidizing inorganic compounds [35, 36] and a wide range of natural and xenobiotic organic contaminants including proteins [37], catechol [38], quinines [39], polyphenols [40], aromatic amines [41], and phosphonates [42]. However, the use of MnO_x particles has several problems such as self-aggregation and precipitation of NPs due to small size and large surface area, leaching of NPs with treated effluent, and difficulty in separating from the solution [43]. To evade these limitations and to facilitate their recovery and reuse, the assembly of NPs onto various solid organic supports has been proven to be an effective strategy. Due to synergetic effects, these organic-inorganic composites exhibit multifunctionalities compared to the free nanomaterial counterparts. Natural biopolymers including cellulose [44, 45], chitin [46], and chitosan [47, 48] have been investigated as excellent solid organic supports for MnO_x NPs due to their high surface area, low density, environmental friendliness, relative abundance, and high fiber strength. Recently, biopolymer-based inorganic-organic composites have been utilized for oxidation processes in dye removal [45, 46]. Polysaccharides such as guar gum (GG) and starch have also been studied in wastewater treatments as flocculants and adsorption agents [49–52]. In contrast to long-chain polymers such as cellulose, chitin, or chitosan, polysaccharides have very high swelling capacities because of the hydrophilic nature of repeating polysaccharide units. Interestingly, polysaccharides can form water-induced interlinked networks during the adsorption permitting fast diffusion of pollutants. However, the utilization of polysaccharides as supporting matrices for NPs has not been extensively investigated.

GG is a naturally occurring polysaccharide derived from the seeds of the guar plant *Cyamopsis tetragonolobus* (cluster bean) which is made up of a linear backbone of β-(1,4)-linked D-mannose units and with the presence of randomly attached α-1,6-linked galactose units as side chains (see Figure 1). These galactose units in the GG facilitate its solubility in water. GG is also a biodegradable, renewable, nontoxic, low-cost, and readily abundant material and has been used in a range of applications including water

treatment [49], food [53], pharmaceutical [54], drug delivery [55], hydraulic fracturing [56], and textile printing [57]. Borax is an effective cross-linker for polysaccharides having hydroxyl functional groups where the borax ions hold the polymer chains together by both physical and chemical linkages [58]. Consequently, the polysaccharide networks form a three-dimensional hydrogel structure extending throughout the solution. Cross-linked polymer exhibits much higher adsorption capacities compared to its native form. In the current study, we report on the use of borax-cross-linked guar gum (GGB) as a host for MnO_2 NPs and its ability to remove the model dye MB. GG and GG-based composites have been mainly investigated for adsorptive decolorization in dye wastewater treatments. To the best of our knowledge, this may be the first attempt to utilize GGB-MnO_2 composite for the oxidative decolorization of the organic dye MB.

2. Experimental

2.1. Materials. Guar gum (GG) and borax were purchased from Sigma-Aldrich (Saint Louis, MO). Sodium hydroxide (NaOH, ≥98%), hydrochloric acid (HCl, 37%) potassium permanganate ($KMnO_4$, ≥99%), acetone (C_3H_6O, ≥99.5%), and manganese dioxide (MnO_2, 85%) were purchased from Fisher Scientific (Pittsburgh, PA). Methylene blue was purchased from ACROS (Morris Plains, NJ). Distilled water was purchased from AquaOne (Amarillo, TX).

2.2. Synthesis of Borax-Cross-Linked Guar Gum Composite. Borax-cross-linked guar gum (abbreviated as GGB) composite was prepared using a previously described method [49]. In a typical synthesis, 1 g of guar gum powder was completely dispersed in 80 mL of distilled water. Then, the solution was kept at room temperature (RT) for 2 h to hydrate and achieve maximum viscosity. 0.2 g of cross-linker borax (20% weight of GG) was separately dissolved in 60 mL of distilled water and added to the GG solution. The mixture was mechanically stirred at RT for 30 min and left for another 4 h without any mechanical stirring. The resulting yellow-color material is the borax-cross-linked guar hydrogel. This synthesized hydrogel was crushed and gently washed with distilled water to remove unreacted borax. Then, the crushed hydrogel was soaked in acetone solution overnight for dehydration. Dehydrated hydrogels were filtered and kept in the oven at 45°C until a constant weight is attained.

2.3. Synthesis of Borax-Cross-Linked Guar Gum-Manganese Dioxide (GGB-MnO_2) Composite. GGB-MnO_2 composite was synthesized using a modified literature method [46]. First, 6.75 mL of 0.25 mol·L^{-1} alkaline permanganate (molar ratio = 1 : 1 $KMnO_4$: NaOH) solution was mixed with 100 mL of distilled water. GGB (1 g) was added to the solution and mechanically stirred with a stirring speed of 500 rpm at RT overnight to obtain in situ-grown GGB-MnO_2 composite. The brown-color composite was thoroughly washed with distilled water to remove unreacted residuals. Finally, the composite was dispersed in distilled water by constant stirring with a stirring speed of 500 rpm. The sample was kept wet to avoid irreversible agglomeration of the hybrid [45]. The solid content of the wet slurry was 60% (*w*/*w*).

The mechanism for the formation of MnO_2 from the reaction between various polysaccharides and $KMnO_4$ has been previously reported [59, 60]. During this reaction, permanganate ion acts as a strong oxidizing agent and involves the oxidation of GG [59, 60]. The overall reaction mechanism involves the formation of keto-GG and MnO_2 nanoparticles as final products. The generation of MnO_2 occurs via two steps: (1) formation of a transient manganese (VI) species and its gradual build up in the solution and (2) a slow decay of the transient species to generate MnO_2 nanoparticles [60]. These particles then deposit and form a thin layer of MnO_2 on the surface of guar gum [60]. The final color of the GGB-MnO_2 composite is brown.

2.4. Ultraviolet-Visible (UV-Vis) Spectrophotometry. UV-Vis spectrophotometric measurements were conducted using a PerkinElmer Lambda 650 spectrophotometer running with PerkinElmer UV WinLab software. All data were analyzed using Microcal Origin version 8.0.

2.5. pH Measurements. pH measurements were carried out at RT using a Fisher Scientific™ accumet™ AB15 Plus pH meter equipped with benchtop stirring probe. The electrode was filled with a 3 M saturated KCl solution (pH 7) and standardized with RICCA precision reference standard solutions at pH 4, 7, and 12. Solution pH was adjusted using HCl (0.10 M) or NaOH (0.05 M) solutions as necessary.

2.6. Decolorization of Methylene Blue (MB). Decolorization of MB was studied using UV-Vis spectroscopy. In a typical experiment, 100 mg of wet GGB-MnO_2 composite (60% (*w*/*w*) solid) was added to a 100 mL beaker containing 50 mL of 30 mg/L MB solution (note that the composite was kept in the wet form in order to prevent the aggregation of small nanoparticles during the drying). The solution was magnetically stirred with a stirring speed of 500 rpm and at predetermined time intervals (30 sec, 1 min, and 2 min at pH 4, 7, and 10, respectively); an aliquot of MB solution (3 mL) was suctioned off and filtered through 0.20 μm syringe filter. Then, the concentrations of the solutions were measured at absorbance maxima, λ_{max} = 664 nm. For comparison purposes, control experiments were also conducted in parallel with 100 mg of GGB and 100 mg of bare MnO_2 under the same experimental setup as described above. The final concentration of MB was determined using a calibration plot (see Figure S1, Supplementary Materials). The same experiment was repeated three times. Reported decolorization efficiencies are the average values of at least three independent measurements.

2.7. Recycling Experiment. Recycling experiments were conducted at pH 4. After the first cycle, the GGB-MnO_2 composite was filtered and thoroughly washed with distilled water several times and then dried in the oven at 60°C for 5 h. The dried composite was reused for decolorization with a MB concentration of 30 mg/L.

2.8. Fourier-Transform Infrared (FTIR) Spectroscopy. FTIR spectroscopy of the GG, GGB, and dry GGB-MnO_2 samples was recorded using a PerkinElmer Spectrum-400 FTIR spectrometer equipped with a universal attenuated total reflectance (UATR) accessory (PerkinElmer, Waltham, MA). All FTIR spectra were collected at a spectral resolution of 4 cm^{-1}, with 32 coadded scans in the wavenumber range of 4000 to 650 cm^{-1}. The spectra were analyzed using PerkinElmer Spectrum software.

2.9. X-Ray Diffraction (XRD) Analysis. The wide-angle powder X-ray diffraction patterns of the samples were recorded on a SmartLab XRD system (Rigaku Corporation, Model HD2711N) with CuK_α radiation ($\lambda = 1.541867$ Å). The accelerating voltage and tube current used were 40 kV and 44 mA, respectively. A continuous scanning was performed at a scan speed of 2°/min, and the 2θ ranged from 10° to 70°.

2.10. Thermogravimetric Analysis (TGA). Thermogravimetric (TG) analysis of GG, GGB, and GGB-MnO_2 were obtained using a PerkinElmer Pyris1TGA instrument (PerkinElmer, Waltham, MA) equipped with a 20-sample autosampler. TG profiles were recorded in an inert nitrogen atmosphere (20 mL/min) from 37°C to 600°C with a constant heating rate of 10°C/min using a high-resolution mode. All data were analyzed using Pyris Data Analysis software.

2.11. Scanning Electron Microscopy (SEM). The morphology of GG, GGB, and GGB-MnO_2 was studied on a Hitachi S-4700 field emission scanning electron microscope (FESEM) equipped with a GENE-SIS4000 energy-dispersive X-ray (EDX) spectroscopy. Resolutions of 1.5 nm at 15 kV and 2.5 at 2 kV can be achieved at 12 mm and 3 nm working distance, respectively.

All samples were conditioned in an environmentally controlled laboratory maintained at a relative humidity of 65 ± 2 % and temperature of 21 ± 1°C for at least 48 h prior to their characterization.

3. Results and Discussion

3.1. XRD Studies. XRD studies were performed to investigate the crystalline properties of GG, GGB, and GGB-MnO_2 samples. All samples display different behaviors in the crystalline structure. XRD patterns of GG, GGB, and GGB-MnO_2 are shown in Figure 2. The GG sample showed a characteristic peak at $2\theta = 20.2°$, and this is in agreement with the diffraction patterns reported for pure GG at $2\theta = 20.2°$ and 72.2° [61]. GGB exhibited slightly shifted broad peak at 18.2° with no distinguishable peaks confirming the formation of cross-linked GG. The GGB-MnO_2 displayed a different XRD pattern with significantly shifted and a reduced main peak. As shown in Figure 2, GGB is low in crystallinity with a broad and weak XRD peak. Upon deposition of MnO_2, the diffraction peak of GGB became much weaker and obscured leading to a highly amorphous structure.

3.2. FESEM and EDX Analysis. FESEM analysis was carried out to observe the surface morphological characteristics of the sample studied. Figure 3 shows the FESEM micrographs

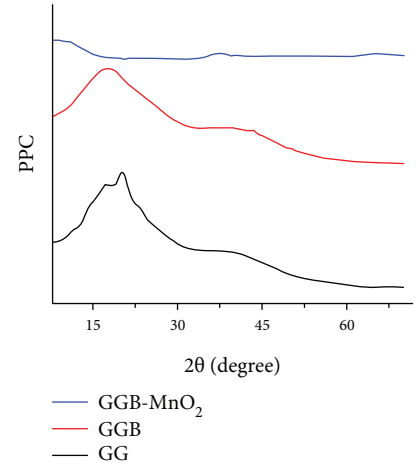

Figure 2: XRD patterns of GG, GGB, and GGB-MnO_2.

of GG, GGB, and GGB-MnO_2 composites and the EDX analysis of GGB-MnO_2 composite. GG powder exhibits a rough surface morphology with no crosslinking between the GG granules, see Figure 3(a). However, GGB composite has a distinct flake-like surface morphology with a smoother surface (see Figure 3(b)). The morphology of GGB-MnO_2 surface is significantly different from GGB. As shown in Figure 3(c), the MnO_2 nanoparticles are completely dispersed and anchored intimately on the surface of the GGB-MnO_2 composite with a broad distribution of the particle size. This suggests strong interactions between the GGB surface and MnO_2 nanoparticles. The particle size of the MnO_2 nanoparticles is in the range of 10–300 nm. The reason for the large particle sizes is due to the formation of aggregates because of irreversible agglomeration of small nanoparticles when the sample is dry. Typically, smaller-sized MnO_2 nanoparticles are expected to exhibit higher catalytic activity as compared to large aggregates. EDX analysis was performed on the GGB-MnO_2 and GGB composites to confirm the presence of B and Mn. As it can be seen in Figure 3(d), the EDX spectrum clearly displays the B, C, O, and Mn peaks at values 0.18, 0.27, 0.52, and 5.8 KeV corresponding to boron, carbon, oxygen, and manganese, respectively. The EDX spectrum of the GGB composite is shown in Figure S2, Supplementary Materials. The EDX data further reveal the formation of borax-cross-linked guar gum (GGB) composite and the deposition of MnO_2 nanoparticles on the surface of the composite.

3.3. FTIR Analysis. FTIR spectra of GG, GGB, and GGB-MnO_2 were recorded to study and compare the changes in their chemical structure. The FTIR spectra of GG, GGB, and GGB-MnO_2 are shown in Figure 4. The presence of a broadband at 3308 cm^{-1} is attributed to –OH stretching band of the polymer, and the peak at 2917 cm^{-1} is assigned to C–H asymmetric stretching vibrations. The peak at 1643 cm^{-1} is associated with –OH bending modes of adsorbed water molecules [49]. The bands at 1015, 1059, and 1147 cm^{-1} are assigned to CH_2 twists, C–O(H) stretching, and C–O–C asymmetric stretching vibrations, respectively [49, 57]. The peak observed at 868 cm^{-1} is due to the skeletal stretching vibrations

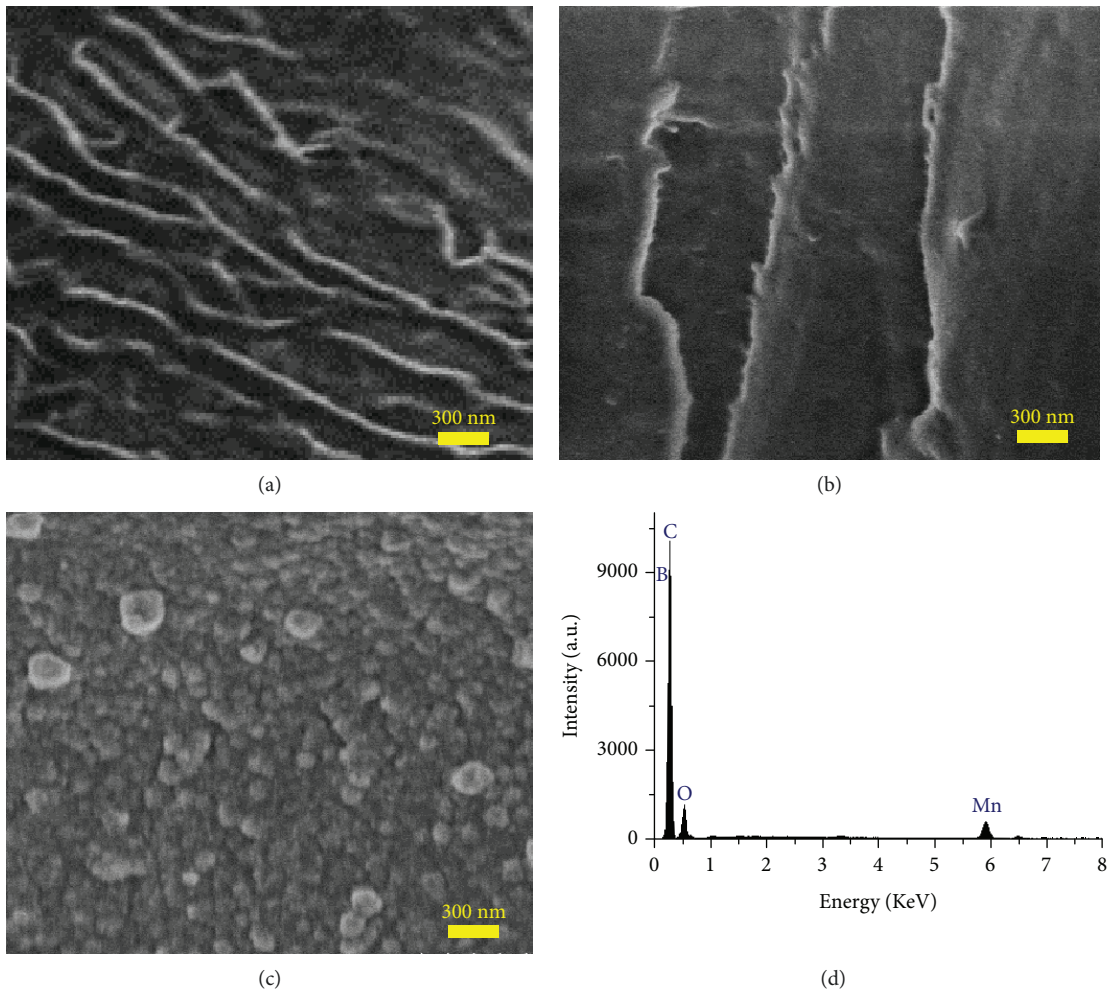

Figure 3: FESEM images of (a) GG, (b) GGB, and (c) GGB-MnO_2 composites. (d) The EDX spectrum of GGB-MnO_2 composite.

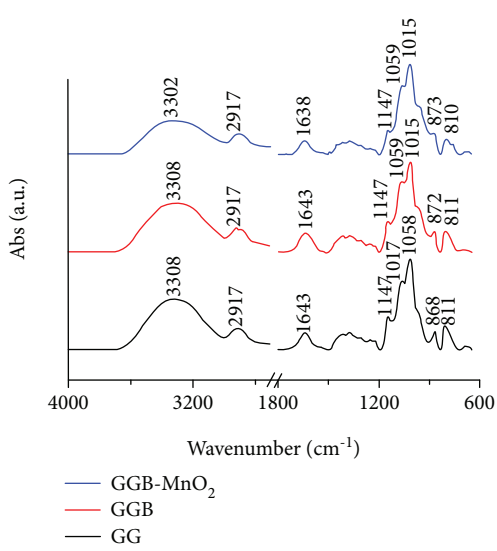

Figure 4: FTIR spectra of GG, GGB, and GGB-MnO_2 samples.

of galactose and mannose units [61, 62]. The –OH stretching band at 3308 cm^{-1} has reduced in both GGB and GGB-MnO_2 composites suggesting the presence of covalent bonding between borax and –OH groups of the galactomannan backbone. The peak 868 cm^{-1} has also decreased in intensity for both GGB and GGB-MnO_2 composites and slightly shifted towards higher wavelength in the GGB-MnO_2 spectrum. This is due to the physical and chemical interaction of –OH groups with borax. The similar spectral pattern for all samples indicates that the chemical structure of guar gum is retained during the synthesis of both GGB and GGB-MnO_2 composites.

3.4. TG Analysis. The thermal stability of the GG, GGB, and GGB-MnO_2 samples was studied by TGA (see Figure 5(a)). TG profiles were obtained to determine the thermal stability of the samples studied and identify their applicability at higher temperatures. Two distinct weight loss regions were observed for pure GG. The initial weight loss region (35–150°C) is attributed to the removal of physically adsorbed water. The second region (150–600°C) is related to the thermal decomposition of the polysaccharide. Both GGB and GGB-MnO_2 samples exhibited three distinct weight loss regions. In the first temperature range of 35–150°C, the

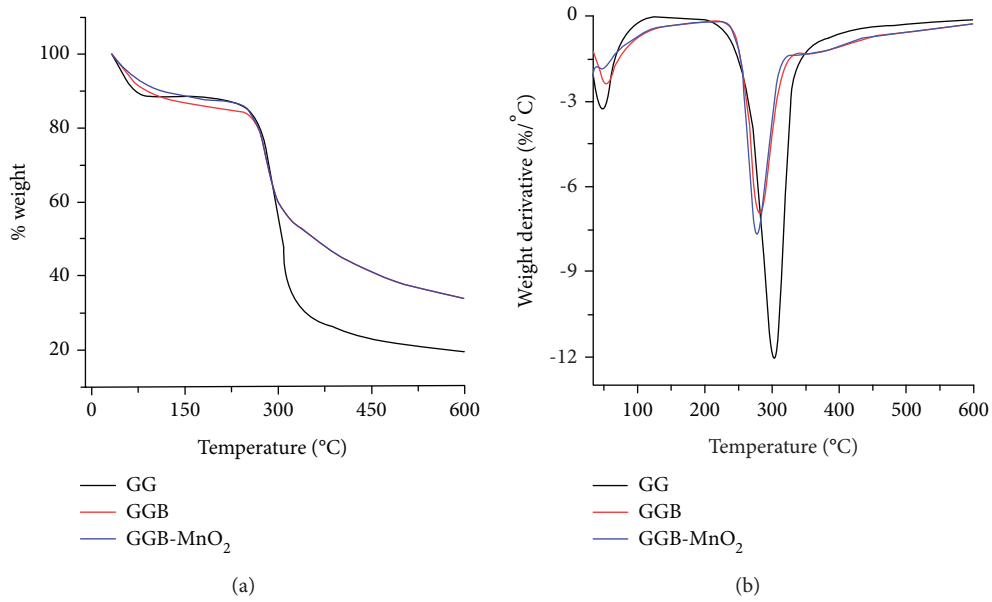

Figure 5: (a) TG and (b) DTG profiles of GG, GGB, and GGB-MnO_2 samples.

weight loss is attributed to the removal of adsorbed moisture. The major weight loss in the region (150–310°C) is assigned to the decomposition of the polysaccharide backbone. The small weight loss above 310°C (310–600°C) is due to the degradation of the cross-linked bonds between borax and hydroxyl groups of the guar side chains. The presence of a third weight loss region for both GGB and GGB-MnO_2 is an indication of the cross-linking between guar and borax. The differential thermogravimetric (DTG) profiles generated form TG results are shown in Figure 5(b). The DTG curves for GG, GGB, and GGB-MnO_2 show peaks at 302, 281, and 277°C, respectively. Our results suggest that the thermal stability is similar for both GGB and GGB-MnO_2; however, it is slightly lowered than pure GG due to the decrease in the crystallinity upon dissolution and crosslinking with borax.

3.5. Decolorization of MB. The decolorization of MB by GGB-MnO_2 was investigated using UV-Vis spectroscopy. Figure 6 shows the UV-Vis spectra as a function of time for MB solution (30 mg/L) treated with GGB-MnO_2 composite (1.2 g/L) at pH 7 (RT). The absorbance of the MB decreases rapidly as a function of time over the entire wavelength range. Interestingly, no additional peaks with any isosbestic points or shift in the peak positions were observed. This suggests that no intermediate or additional species were formed during the reaction between MnO_2 nanoparticles and MB. Therefore, these spectral changes are associated with the loss of conjugation in the heterocyclic aromatic structure, which is responsible for intense π to π^* electronic transitions. A similar experiment was conducted in parallel with GGB and bare MnO_2 particles. These control experiments show that the decrease in the absorbance of MB is significantly less as compared to GGB-MnO_2 composite (see Figures S3 and S4, Supplementary Materials).

The absorbance at 664 nm was used to evaluate the degree of decolorization. Figure 7 shows a plot of the

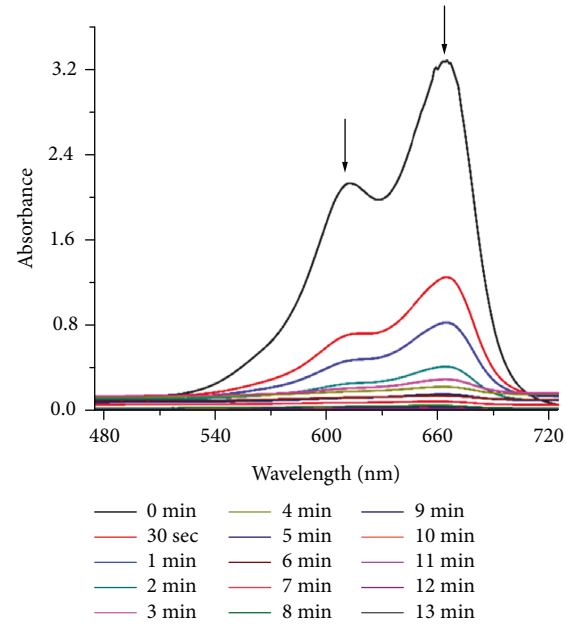

Figure 6: UV-Vis spectra for MB solution (30 mg/L) in the presence of GGB-MnO_2 composite (1.2 g/L) as a function of time at pH 7 (RT).

normalized concentration (C/C_0) of MB as a function of time at pH 7 (RT) and also compares the efficiency of MB decolorization by GGB-MnO_2, GGB, and bare MnO_2. As expected, the decolorization process of MB solution is extremely fast in the presence of GGB-MnO_2 composite. The MB (30 mg/L) solution is 89.6 ± 1.51% decolored over 3 min and almost completely decolored after a 13 min contact time, showing its effectiveness and efficiency. However, the degree of MB decolorization is 24.3 ± 1.72% for GGB and is 36.3 ± 0.80% for bare MnO_2 in 13 min under

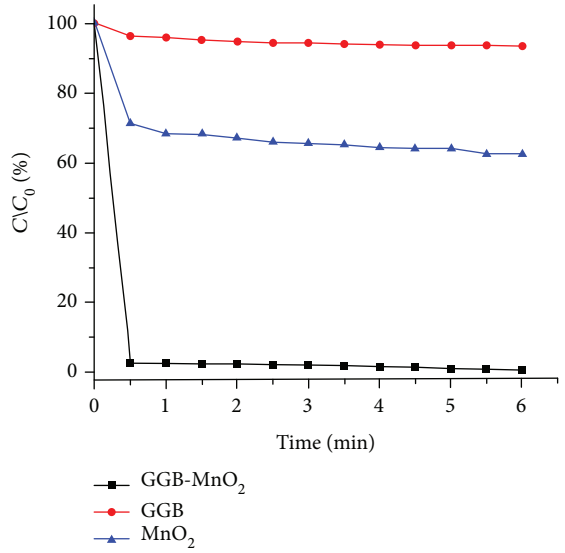

Figure 7: Plot of normalized concentration (C/C_0) versus time for the decolorization of MB (30 mg/L) in the presence of GGB-MnO_2 composite (1.2 g/L), GGB composite (2 g/L), and MnO_2 (2 g/L) at pH 7 (RT), respectively.

stirring. As can be seen in Figure 7, the GGB-MnO_2 hybrid exhibited a remarkably higher performance compared to GGB and bare MnO_2. This is due to the high surface area of the composite material providing more active sites for dye adsorption. We previously showed increased surface area for MnO_2-based composite materials as compared to the starting materials using nitrogen adsorption studies [46].

3.6. Decolorization Mechanism. The mechanism for the decomposition of the organic compounds by MnO_2 has been well established [46, 63]. Generally, the degradation is an adsorption-oxidation-desorption process which occurs via a surface mechanism [63]. The organic compounds are first adsorbed onto the surface of MnO_2 to form a surface precursor complex. Then, an electron transfer reaction occurs between the organic compound where Mn(IV) is reduced to Mn(II) while the organic reductant is being oxidized. During the reduction process of MnO_2, strong oxidizing radicals such as hydroxyl ($OH^{\bullet}$) are also formed [39, 64]. These radicals undergo a cascade of reactions, leading to complete destruction of the chromophore. Moreover, this oxidative degradation is much favorable at low pH conditions [33]. Importantly, Mn(II) can be oxidized to Mn(IV) and precipitated as manganese hydrated oxide; hence, MnO_x nanoparticles act as an active catalyst during the oxidative decolorization [63]. The main products of MB mineralization include mainly SO_4^{2-} and other inorganic ions, such as Cl^-, NO_3^-, CO_2, and H_2O [46].

3.7. Effect of pH on the MB Decolorization. The pH of the solution plays a vital role in the degradation of organic dyes. Therefore, the influence of pH on the degree of decolorization of MB (30 mg/L) by GGB-MnO_2 (1.2 g/L) was investigated at pH 4 and pH 10, and the data are shown in Figures S5 and S6, Supplementary Materials. Plots of the normalized concentration (C/C_0) of MB as a function of time at pH 4 and 10 (RT) are shown in Figures S5 and S6, Supplementary Materials. Our data suggest that 97.5% of MB was decolored in 30 s and was completely decolored within 6 min at pH 4, whereas 99.1% of MB was decolored within 40 min at pH 10. The degree of decolorization for GGB composite and bare MnO_2 at pH 4 and 10 is 6.4, 37.5% within 6 min, and 30.4, 49.7% within 40 min, respectively (see Figures S5 and S6, Supplementary Materials). The reaction time for the decolorization of MB by GGB-MnO_2 increases with the increase in the pH. At alkaline pH, the cross-linked guar gets more negative charge, facilitating higher dye adsorption due to the electrostatic attraction between the cationic MB^+ and the borate ions and the electron-rich hydroxyl groups of GG. The pH has been found to exert double-edged effects on the decolorization of organics by MnO_x [34]. The zero point of charge (pH_{zpc}) of MnO_2 is 4.7 [63]. Therefore, the oxidizing ability of MnO_2 increases with decreasing pH. Theoretically, at lower pH ($pH<pH_{zpc}$) the surface layer of MnO_2 is positively charged due to protonation. The positive charge on the surface layer would not favor the interaction between cationic MB^+ ions and MnO_2 due to the electrostatic repulsion and increased competition between H^+ and MB^+ ions. Hence, the increase in the pH ($pH>pH_{zpc}$) would enhance the dye adsorption because of the ionization and increased electrostatic interaction. Oppositely, the increase in pH suppresses the oxidizing power of MnO_2 [45]. Our results show that decolorization at pH 4 is more effective than that at pH 10. The reason could be that the acidic pH enhances the reduction potential of MnO_2 and thus could compensate and even predominate over MB adsorption via electrostatic effects.

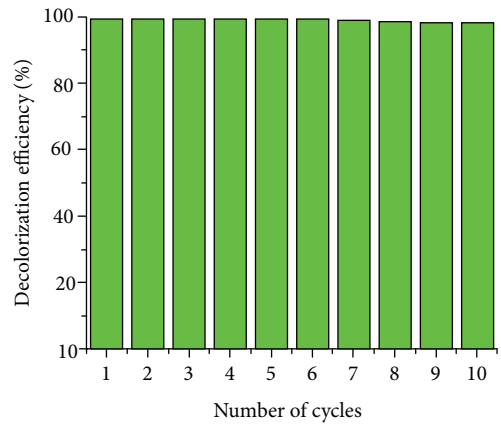

Figure 8: Recyclability of the GGB-MnO_2 composite at pH 4 (RT).

3.8. Recycling Experiment. The reusability of the GGB-MnO_2 composite was evaluated over a number of adsorption-oxidation-desorption cycles. Figure 8 shows the cycle stability of GGB-MnO_2 composite on the decolorization of MB at pH 4 (RT). Our results show an extremely high degree of decolorization of above 98% for 10 cycles. This reveals a long-term stability, high performance, and efficacy of the GGB-MnO_2 composite for effective removal of MB. One of the main reasons for the high stability and reusability

of this material is due to the catalytic oxidative decolorization mechanism where the MnO_2 nanoparticles that regenerated during the dye degradation process continued to react with the dye. Another reason is the stability of MnO_2 particles anchored on the borax-cross-linked guar gum (GGB) composite. Evidently, the GGB composite plays an imperative role in stabilizing MnO_2 nanoparticles and preventing the agglomeration which suppresses the catalytic activity during the repeated oxidative decolorization process. Besides, the rich hydroxyl groups in GG with high chelating ability also help to stabilize the nanoparticles and keep them from leaching out.

Several studies have been reported on guar gum-based composites for the removal of organic dyes from aqueous solutions. For instance, Shruthi et al. studied the efficiency of the guar gum-grafted acrylic acid/nanoclay composite on the adsorption of crystal violet dye and reported that it requires at least three hours to reach the maximum dye adsorption capacity of 12.5 mg/g [65]. Saxena and Sharma investigated the adsorption and kinetic studies on the removal of methyl red dye from aqueous solution using guar gum powder, which showed a monolayer dye adsorption capacity of 66.66 mg/g in three hours at pH 4.2 [66]. Pal and coworkers synthesized guar gum graft-poly(acrylamide)/silica hybrid nanocomposite and showed adsorption capacities of 579.01 mg/g within 40 min and 233.24 mg/g within 30 min for reactive blue and Congo red dyes [67]. Magnetic guar gum-grafted multiwall carbon nanotube iron oxide (GG-MWCNT-Fe_2O_3) composite was investigated for the removal of neutral red (NR) and methylene blue (MB) by Yan and coworkers [68]. They reported maximum adsorption of NR, and MB reached 89.85 mg/L at 20 min and 61.92 at 120 min [68]. Sharma et al. synthesized guar gum-polyacrylic acid-based cross-linked (cl) hydrogels (GG-cl-poly AA) with interpenetrating networks (IPNs) of polyaniline and investigated their percent adsorption of MB with respect to contact time, adsorbent dosage, pH, and temperature [51]. Gupta and coworkers studied the removal of MB by guar gum-cerium(IV) tungstate nanocomposite (GG/CTNC) and showed that an optimum adsorption of MB onto GG/CTNC is 16 mg/g over 120 min [69]. Borax-cross-linked guar gum hydrogels were developed and investigated for the removal of aniline blue dye by Thombare et al. [49] where they showed a maximum decolorizing efficiency of 94% within 60 min [49].

Among those studies reported on guar-based materials, adsorption method has been preferred for the decolorization of organic dyes because of its simplicity and low cost. However, the adsorption method is associated with many drawbacks including high regeneration cost, loss of adsorption efficiency after regeneration, the hazardous nature of the used adsorbent, and require longer times. Albeit oxidative decolorization processes have distinct advantages over adsorptive methods, there is scant literature about the utilization of guar gum-based materials for oxidative decolorization processes. Importantly, our results show that GGB-MnO_2 composite has higher decolorization efficiency and fast reaction time as compared to previous studies reported on GG-based materials used for adsorption. Therefore, due to fast response time, zero accumulation of organics, reusability, and simplicity of the synthesis route, the low cost and green nature of GGB-MnO_2 composite make this material a promising candidate for large-scale dye removal from industrial wastewater.

4. Conclusions

This work reports the synthesis of borax-cross-linked guar gum-manganese dioxide (GGB-MnO_2) composite for efficient oxidative decolorization of methylene blue (MB) dye using UV-Vis spectroscopy. The presence of MnO_2 on the GGB composite showed superior decolorization activity and degradation of MB. The reaction times for the complete oxidative decolorization efficiency (<99%) of MB (30 mg/L) onto GGB-MnO_2 (1.2 g/L) are 6, 13, and 40 min at pH 4, 7, and 10, respectively. The reusability studies showed that the GGB-MnO_2 is stable even after 10 adsorption-oxidation-desorption cycles. Because of the environmentally benign synthesis route and dual adsorptive and catalytic oxidative decolorization mechanism and efficiency, GGB-MnO_2 composite exhibits potential for the remediation of industrial dye wastewater.

Data Availability

The data used to support the findings of this study are available from the corresponding author upon request.

Conflicts of Interest

The authors declare that they have no conflict of interest.

Acknowledgments

The authors would like to thank Dr. Yang Hu for conducting the EDX analysis and the Fiber and Biopolymer Research Institute (FBRI) at Texas Tech University.

Supplementary Materials

Figure S1: the calibration plot for methylene blue (MB) at 664 nm. The concertation of the MB solution was determined using the calibration plot. Figure S2: the EDX spectrum of borax-cross-linked guar gum (GGB) composite in the absence of MnO_2. The EDX spectrum clearly displays the peaks at 0.18, 0.27, and 0.52 KeV corresponding to boron, carbon, and oxygen, respectively. Figure S3: the UV-Vis spectra over 13 min for MB solution (30 mg/L) treated with GGB (1.2 g/L) at pH 7.00 (RT). The absorbance of the MB decreases as a function of time over the entire wavelength range. Figure S4: the UV-Vis spectra over 13 min for MB solution (30 mg/L) treated with bare MnO_2 particles (1.2 g/L) at pH 7.00 (RT). The absorbance of the MB decreases as a function of time over the entire wavelength range. Figure S5: a plot of the normalized concentration (C/C_0) of MB as a function of time at pH 4.00 (RT) and also a comparison of the efficiency of MB decolorization by GGB-MnO_2, GGB, and bare MnO_2. The degree of decolorization for GGB-MnO_2, GGB, and bare MnO_2 at pH 4.00 after

6 min is 99.9, 6.4, and 37.5%, respectively. Figure S6: a plot of the normalized concentration (C/C_0) of MB as a function of time at pH 10.00 (RT) and also a comparison of the efficiency of MB decolorization by GGB-MnO_2, GGB, and bare MnO_2. The degree of decolorization for GGB-MnO_2, GGB, and bare MnO_2 at pH 4.00 after 40 min is 99.1, 30.4, and 49.7%, respectively. *(Supplementary Materials)*

References

[1] F. M. D. Chequer, G. A. R. de Oliveira, E. R. A. Ferraz, J. C. Cardoso, M. V. B. Zanoni, and D. P. de Oliveira, "Textile dyes: dyeing process and environmental impact," in *Eco-Friendly Textile Dyeing and Finishing, Chapter 06*, M. Günay, Ed., pp. 151–163, InTech, Rijeka, 2013.

[2] Y. Zhou, S. Fu, H. Liu, S. Yang, and H. Zhan, "Removal of methylene blue dyes from wastewater using cellulose-based superadsorbent hydrogels," *Polymer Engineering and Science*, vol. 51, no. 12, pp. 2417–2424, 2011.

[3] F. C. F. Low, T. Y. Wu, C. Y. Teh, J. C. Juan, and N. Balasubramanian, "Investigation into photocatalytic decolorisation of CI reactive black 5 using titanium dioxide," *Coloration Technology*, vol. 128, no. 1, pp. 44–50, 2012.

[4] L. Liu, B. Zhang, Y. Zhang et al., "Simultaneous removal of cationic and anionic dyes from environmental water using montmorillonite-pillared graphene oxide," *Journal of Chemical & Engineering Data*, vol. 60, no. 5, pp. 1270–1278, 2015.

[5] G. Moussavi and M. Mahmoudi, "Removal of azo and anthraquinone reactive dyes from industrial wastewaters using MgO nanoparticles," *Journal of Hazardous Materials*, vol. 168, no. 2-3, pp. 806–812, 2009.

[6] L. Zhang, Y. Nie, C. Hu, and X. Hu, "Decolorization of methylene blue in layered manganese oxide suspension with H_2O_2," *Journal of Hazardous Materials*, vol. 190, no. 1–3, pp. 780–785, 2011.

[7] M. Rafatullah, O. Sulaiman, R. Hashim, and A. Ahmad, "Adsorption of methylene blue on low-cost adsorbents: a review," *Journal of Hazardous Materials*, vol. 177, no. 1–3, pp. 70–80, 2010.

[8] Y. Li, Q. Du, T. Liu et al., "Comparative study of methylene blue dye adsorption onto activated carbon, graphene oxide, and carbon nanotubes," *Chemical Engineering Research and Design*, vol. 91, no. 2, pp. 361–368, 2013.

[9] M. X. Zhu, L. Lee, H. H. Wang, and Z. Wang, "Removal of an anionic dye by adsorption/precipitation processes using alkaline white mud," *Journal of Hazardous Materials*, vol. 149, no. 3, pp. 735–741, 2007.

[10] A. Alaoui, K. El Kacemi, K. El Ass, S. Kitane, and S. El Bouzidi, "Activity of Pt/MnO_2 electrode in the electrochemical degradation of methylene blue in aqueous solution," *Separation and Purification Technology*, vol. 154, pp. 281–289, 2015.

[11] Y. J. Chan, M. F. Chong, C. L. Law, and D. G. Hassell, "A review on anaerobic–aerobic treatment of industrial and municipal wastewater," *Chemical Engineering Journal*, vol. 155, no. 1-2, pp. 1–18, 2009.

[12] M. Işık and D. T. Sponza, "Biological treatment of acid dyeing wastewater using a sequential anaerobic/aerobic reactor system," *Enzyme and Microbial Technology*, vol. 38, no. 7, pp. 887–892, 2006.

[13] H. Patel and R. T. Vashi, "Removal of Congo Red dye from its aqueous solution using natural coagulants," *Journal of Saudi Chemical Society*, vol. 16, no. 2, pp. 131–136, 2012.

[14] C. Y. Teh, P. M. Budiman, K. P. Y. Shak, and T. Y. Wu, "Recent advancement of coagulation–flocculation and its application in wastewater treatment," *Industrial and Engineering Chemistry Research*, vol. 55, no. 16, pp. 4363–4389, 2016.

[15] G. Ciardelli, L. Corsi, and M. Marcucci, "Membrane separation for wastewater reuse in the textile industry," *Resources, Conservation and Recycling*, vol. 31, no. 2, pp. 189–197, 2001.

[16] J. Huang, L. Peng, G. Zeng et al., "Evaluation of micellar enhanced ultrafiltration for removing methylene blue and cadmium ion simultaneously with mixed surfactants," *Separation and Purification Technology*, vol. 125, pp. 83–89, 2014.

[17] K. Zhang, F. J. Zhang, M. L. Chen, and W. C. Oh, "Comparison of catalytic activities for photocatalytic and sonocatalytic degradation of methylene blue in present of anatase TiO_2–CNT catalysts," *Ultrasonics Sonochemistry*, vol. 18, no. 3, pp. 765–772, 2011.

[18] R. S. Dariani, A. Esmaeili, A. Mortezaali, and S. Dehghanpour, "Photocatalytic reaction and degradation of methylene blue on TiO_2 nano-sized particles," *Optik*, vol. 127, no. 18, pp. 7143–7154, 2016.

[19] F. L. Rosario-Ortiz, E. C. Wert, and S. A. Snyder, "Evaluation of UV/H_2O_2 treatment for the oxidation of pharmaceuticals in wastewater," *Water Research*, vol. 44, no. 5, pp. 1440–1448, 2010.

[20] S. Raghu and C. Ahmed Basha, "Chemical or electrochemical techniques, followed by ion exchange, for recycle of textile dye wastewater," *Journal of Hazardous Materials*, vol. 149, no. 2, pp. 324–330, 2007.

[21] L. Zhuang, S. Zhou, Y. Yuan, M. Liu, and Y. Wang, "A novel bioelectro-Fenton system for coupling anodic COD removal with cathodic dye degradation," *Chemical Engineering Journal*, vol. 163, no. 1-2, pp. 160–163, 2010.

[22] H. Lim, J. Lee, S. Jin, J. Kim, J. Yoon, and T. Hyeon, "Highly active heterogeneous Fenton catalyst using iron oxide nanoparticles immobilized in alumina coated mesoporous silica," *Chemical Communications*, no. 4, pp. 463–465, 2006.

[23] C. L. Hsueh, Y. H. Huang, C. C. Wang, and C. Y. Chen, "Degradation of azo dyes using low iron concentration of Fenton and Fenton-like system," *Chemosphere*, vol. 58, no. 10, pp. 1409–1414, 2005.

[24] M. Matheswaran and T. Raju, "Destruction of methylene blue by mediated electrolysis using two-phase system," *Process Safety and Environment Protection*, vol. 88, no. 5, pp. 350–355, 2010.

[25] Y. Deng and R. Zhao, "Advanced oxidation processes (AOPs) in wastewater treatment," *Current Pollution Reports*, vol. 1, no. 3, pp. 167–176, 2015.

[26] J. L. Wang and L. J. Xu, "Advanced oxidation processes for wastewater treatment: formation of hydroxyl radical and application," *Critical Reviews in Environmental Science and Technology*, vol. 42, no. 3, pp. 251–325, 2012.

[27] C. Y. Teh, T. Y. Wu, and J. C. Juan, "An application of ultrasound technology in synthesis of titania-based photocatalyst for degrading pollutant," *Chemical Engineering Journal*, vol. 317, pp. 586–612, 2017.

[28] L. V. Trandafilović, D. J. Jovanović, X. Zhang, S. Ptasińska, and M. D. Dramićanin, "Enhanced photocatalytic degradation of methylene blue and methyl orange by ZnO:Eu nanoparticles," *Applied Catalysis B: Environmental*, vol. 203, pp. 740–752, 2017.

[29] X. Wan, M. Yuan, S.-l. Tie, and S. Lan, "Effects of catalyst characters on the photocatalytic activity and process of NiO nanoparticles in the degradation of methylene blue," *Applied Surface Science*, vol. 277, pp. 40–46, 2013.

[30] R. Saravanan, S. Joicy, V. K. Gupta, V. Narayanan, and A. Stephen, "Visible light induced degradation of methylene blue using CeO_2/V_2O_5 and CeO_2/CuO catalysts," *Materials Science and Engineering: C*, vol. 33, no. 8, pp. 4725–4731, 2013.

[31] M. Behera and G. Giri, "Inquiring the photocatalytic activity of cuprous oxide nanoparticles synthesized by a green route on methylene blue dye," *International Journal of Industrial Chemistry*, vol. 7, no. 2, pp. 157–166, 2016.

[32] C. K. Remucal and M. Ginder-Vogel, "A critical review of the reactivity of manganese oxides with organic contaminants," *Environmental Science: Processes & Impacts*, vol. 16, no. 6, pp. 1247–1266, 2014.

[33] H. Sun, Y. Shang, K. Xu, Y. Tang, J. Li, and Z. Liu, "MnO_2 aerogels for highly efficient oxidative degradation of rhodamine B," *RSC Advances*, vol. 7, no. 48, pp. 30283–30288, 2017.

[34] M.-X. Zhu, Z. Wang, S.-H. Xu, and T. Li, "Decolorization of methylene blue by δ-MnO_2-coated montmorillonite complexes: emphasizing redox reactivity of Mn-oxide coatings," *Journal of Hazardous Materials*, vol. 181, no. 1–3, pp. 57–64, 2010.

[35] R. Dai, J. Liu, C. Yu, R. Sun, Y. Lan, and J. D. Mao, "A comparative study of oxidation of Cr(III) in aqueous ions, complex ions and insoluble compounds by manganese-bearing mineral (birnessite)," *Chemosphere*, vol. 76, no. 4, pp. 536–541, 2009.

[36] V. Q. Chiu and J. G. Hering, "Arsenic adsorption and oxidation at manganite surfaces. 1. Method for simultaneous determination of adsorbed and dissolved arsenic species," *Environmental Science & Technology*, vol. 34, no. 10, pp. 2029–2034, 2000.

[37] M. Altaf and D. Jaganyi, "Oxidative degradation of l-histidine by manganese dioxide (MnO_2) nano-colloid in $HClO_4$ medium with/without using TX-100 catalyst: a kinetic approach," *RSC Advances*, vol. 6, no. 103, pp. 101162–101170, 2016.

[38] C. J. Matocha, D. L. Sparks, J. E. Amonette, and R. K. Kukkadapu, "Kinetics and mechanism of birnessite reduction by catechol," *Soil Science Society of America Journal*, vol. 65, no. 1, pp. 58–66, 2001.

[39] A. T. Stone and J. J. Morgan, "Reduction and dissolution of manganese(III) and manganese(IV) oxides by organics. 1. Reaction with hydroquinone," *Environmental Science & Technology*, vol. 18, no. 6, pp. 450–456, 1984.

[40] R. A. Petrie, P. R. Grossl, and R. C. Sims, "Oxidation of pentachlorophenol in manganese oxide suspensions under controlled E_h and pH environments," *Environmental Science & Technology*, vol. 36, no. 17, pp. 3744–3748, 2002.

[41] S. Laha and R. G. Luthy, "Oxidation of aniline and other primary aromatic amines by manganese dioxide," *Environmental Science & Technology*, vol. 24, no. 3, pp. 363–373, 1990.

[42] K. A. Barrett and M. B. McBride, "Oxidative degradation of glyphosate and aminomethylphosphonate by manganese oxide," *Environmental Science & Technology*, vol. 39, no. 23, pp. 9223–9228, 2005.

[43] S. M. Maliyekkal, K. P. Lisha, and T. Pradeep, "A novel cellulose–manganese oxide hybrid material by in situ soft chemical synthesis and its application for the removal of Pb(II) from water," *Journal of Hazardous Materials*, vol. 181, no. 1–3, pp. 986–995, 2010.

[44] J. Zeng, S. Liu, J. Cai, and L. Zhang, "TiO_2 immobilized in cellulose matrix for photocatalytic degradation of phenol under weak UV light irradiation," *The Journal of Physical Chemistry C*, vol. 114, no. 17, pp. 7806–7811, 2010.

[45] Y. Wang, X. Zhang, X. He, W. Zhang, X. Zhang, and C. Lu, "In situ synthesis of MnO_2 coated cellulose nanofibers hybrid for effective removal of methylene blue," *Carbohydrate Polymers*, vol. 110, pp. 302–308, 2014.

[46] R. S. Dassanayake, E. Rajakaruna, H. Moussa, and N. Abidi, "One-pot synthesis of MnO_2–chitin hybrids for effective removal of methylene blue," *International Journal of Biological Macromolecules*, vol. 93, Part A, pp. 350–358, 2016.

[47] T. Kamal, M. Ul-Islam, S. B. Khan, and A. M. Asiri, "Adsorption and photocatalyst assisted dye removal and bactericidal performance of ZnO/chitosan coating layer," *International Journal of Biological Macromolecules*, vol. 81, pp. 584–590, 2015.

[48] D. Akin, A. Yakar, and U. Gunduz, "Synthesis of magnetic Fe_3O_4-chitosan nanoparticles by ionic gelation and their dye removal ability," *Water Environment Research*, vol. 87, no. 5, pp. 425–436, 2015.

[49] N. Thombare, U. Jha, S. Mishra, and M. Z. Siddiqui, "Borax cross-linked guar gum hydrogels as potential adsorbents for water purification," *Carbohydrate Polymers*, vol. 168, pp. 274–281, 2017.

[50] M. S. Zafar, M. Tausif, M. Mohsin, S. W. Ahmad, and M. Zia-ul-Haq, "Potato starch as a coagulant for dye removal from textile wastewater," *Water, Air, and Soil Pollution*, vol. 226, no. 8, p. 244, 2015.

[51] R. Sharma, B. S. Kaith, S. Kalia et al., "Biodegradable and conducting hydrogels based on guar gum polysaccharide for antibacterial and dye removal applications," *Journal of Environmental Management*, vol. 162, pp. 37–45, 2015.

[52] F. Delval, G. Crini, J. Vebrel, M. Knorr, G. Sauvin, and E. Conte, "Starch-modified filters used for the removal of dyes from waste water," *Macromolecular Symposia*, vol. 203, no. 1, pp. 165–172, 2003.

[53] D. Mudgil, S. Barak, and B. S. Khatkar, "Guar gum: processing, properties and food applications—a review," *Journal of Food Science and Technology*, vol. 51, no. 3, pp. 409–418, 2014.

[54] N. Thombare, U. Jha, S. Mishra, and M. Z. Siddiqui, "Guar gum as a promising starting material for diverse applications: a review," *International Journal of Biological Macromolecules*, vol. 88, pp. 361–372, 2016.

[55] G. Sen, S. Mishra, U. Jha, and S. Pal, "Microwave initiated synthesis of polyacrylamide grafted guar gum (GG-g-PAM)-characterizations and application as matrix for controlled release of 5-amino salicylic acid," *International Journal of Biological Macromolecules*, vol. 47, no. 2, pp. 164–170, 2010.

[56] Y. Lester, T. Yacob, I. Morrissey, and K. G. Linden, "Can we treat hydraulic fracturing flowback with a conventional

biological process? The case of guar gum," *Environmental Science & Technology Letters*, vol. 1, no. 1, pp. 133–136, 2014.

[57] H. Gong, M. Liu, B. Zhang et al., "Synthesis of oxidized guar gum by dry method and its application in reactive dye printing," *International Journal of Biological Macromolecules*, vol. 49, no. 5, pp. 1083–1091, 2011.

[58] G. Bocchinfuso, C. Mazzuca, C. Sandolo et al., "Guar gum and scleroglucan interactions with borax: experimental and theoretical studies of an unexpected similarity," *The Journal of Physical Chemistry B*, vol. 114, no. 41, pp. 13059–13068, 2010.

[59] R. Hassan, A. R. Dahy, S. Ibrahim, I. Zaafarany, and A. Fawzy, "Oxidation of some macromolecules. Kinetics and mechanism of oxidation of methyl cellulose polysaccharide by permanganate ion in acid perchlorate solutions," *Industrial and Engineering Chemistry Research*, vol. 51, no. 15, pp. 5424–5432, 2012.

[60] K. S. Khairou, "Kinetics and mechanism of decomposition of intermediate complex during oxidation of pectate polysaccharide by potassium permanganate in alkaline solutions," *International Journal of Chemical Kinetics*, vol. 35, no. 2, pp. 67–72, 2003.

[61] D. Mudgil, S. Barak, and B. S. Khatkar, "X-ray diffraction, IR spectroscopy and thermal characterization of partially hydrolyzed guar gum," *International Journal of Biological Macromolecules*, vol. 50, no. 4, pp. 1035–1039, 2012.

[62] L. Dai, Z. Long, J. Chen et al., "Robust guar gum/cellulose nanofibrils multilayer films with good barrier properties," *ACS Applied Materials & Interfaces*, vol. 9, no. 6, pp. 5477–5485, 2017.

[63] W. H. Kuan and Y. C. Chan, "pH-dependent mechanisms of methylene blue reacting with tunneled manganese oxide pyrolusite," *Journal of Hazardous Materials*, vol. 239-240, pp. 152–159, 2012.

[64] Y. Ono, T. Matsumura, and S.-i. Fukuzumi, "Electron spin resonance studies on the mechanism of the formation of *p*-benzosemiquinone anion over manganese dioxide," *Journal of the Chemical Society, Perkin Transactions*, vol. 2, no. 11, pp. 1421–1424, 1977.

[65] S. B. Shruthi, C. Bhat, S. P. Bhaskar, G. Preethi, and R. R. N. Sailaja, "Microwave assisted synthesis of guar gum grafted acrylic acid/nanoclay superabsorbent composites and its use in crystal violet dye absorption," *Green and Sustainable Chemistry*, vol. 6, no. 1, pp. 11–25, 2016.

[66] R. Saxena and S. Sharma, "Adsorption and kinetic studies on the removal of methyl red from aqueous solutions using low-cost adsorbent: guargum powder," *International Journal of Scientific & Engineering Research*, vol. 7, no. 3, pp. 675–683, 2016.

[67] S. Pal, A. S. Patra, S. Ghorai et al., "Efficient and rapid adsorption characteristics of templating modified guar gum and silica nanocomposite toward removal of toxic reactive blue and Congo red dyes," *Bioresource Technology*, vol. 191, pp. 291–299, 2015.

[68] L. Yan, P. R. Chang, P. Zheng, and X. Ma, "Characterization of magnetic guar gum-grafted carbon nanotubes and the adsorption of the dyes," *Carbohydrate Polymers*, vol. 87, no. 3, pp. 1919–1924, 2012.

[69] V. K. Gupta, D. Pathania, P. Singh, A. Kumar, and B. S. Rathore, "Adsorptional removal of methylene blue by guar gum–cerium (IV) tungstate hybrid cationic exchanger," *Carbohydrate Polymers*, vol. 101, pp. 684–691, 2014.